Balance of Activity during a Critical Period Tunes a Developing Network

Iain Hunter[1*], Bramwell Coulson[1*], Tom Pettini[2], Jacob J. Davies[1], Jill Parkin[1], Matthias Landgraf[2‡], & Richard A. Baines[1‡].

[1]Division of Neuroscience, School of Biological Sciences, Faculty of Biology, Medicine and Health, University of Manchester, Manchester Academic Health Science Centre, Manchester, M13 9PL, UK.

[2]Department of Zoology, University of Cambridge, Cambridge CB2 3EJ, United Kingdom.

*Joint first authors

‡Joint corresponding authors

Richard Baines: Richard.Baines@manchester.ac.uk

Matthias Landgraf: ml10006@cam.ac.uk

Abstract

Developing neural circuits are influenced by activity and are especially sensitive to changes in activity during critical periods (CPs) of development. Changes occurring during a CP often become 'locked-in' so that they affect the mature network. Indeed, several neurodevelopmental disorders have been linked to excessive activity during such periods. It is, therefore, important to identify those aspects of neural circuit development that are influenced by neural activity during a CP. In this study, we take advantage of the genetic tractability of *Drosophila* to show that activity perturbation during an embryonic CP permanently alters properties of the locomotor circuit. Specific changes we identify include increased synchronicity of motoneuron activity, and greater strengthening of excitatory over inhibitory synaptic drive to motoneurons. These changes are sufficient to reduce network robustness, evidenced by increased sensitivity to induced seizure. We also show that we can rescue these changes when increased activity is mitigated by inhibition provided by mechanosensory neurons. Similarly, we demonstrate a dose-dependent relationship between inhibition experienced during the CP, and the extent to which it is possible to rescue the hyperexcitable phenotype characteristic of the *para*^{bss} mutation. This suggests that developing circuits must be exposed to a properly balanced sum of excitation and inhibition during the CP, to achieve normal mature network function. Our results, therefore, provide novel insight into how activity during a CP shapes specific elements of a circuit, and how activity during this period is integrated to tune neural circuits to the environment in which they will likely function.

Introduction

A developing nervous system is exposed to multiple, and unpredictable, influences that can alter mature circuit function. These include extrinsic and intrinsic factors, such as temperature, light, mechanical stress and/or genetic mutations. Multiple studies have revealed that developing neural networks are most sensitive to neuronal activity during critical periods (CPs) – defined periods in developmental time during which plasticity peaks (Hensch, 2005; Reh *et al.*, 2020; Wong-Riley, 2021). Indeed, work in several model organisms has shown that activity perturbation during a CP often becomes 'locked in' so that once the CP is closed, the mature nervous system remains changed. This was first demonstrated by Hubel and Wiesel (Hubel and Wiesel, 1970) who showed that blocking visual input in kittens, but not in adult cats, caused significant, lasting change in ocular dominance. Thus, visual activity during early life is necessary for normal development of vision. Since these pioneering experiments, CPs have been identified in other networks and across species, which indicates that they are a common phenomenon in the development of neural circuits (Marley and Baines, 2011a; Giachello and Baines, 2015; Golovin *et al.*, 2019; Styr *et al.*, 2019; Hensch and Bilimoria, 2012).

Recent studies posit that aberrant activity during CPs contributes to, and may even cause neurodevelopmental disorders including autism (LeBlanc and Fagiolini, 2011), schizophrenia (Selemon and Zecevic, 2015) and epilepsy (Lybrand *et al.*, 2021). Specifically, this growing body of work suggests that excessive activity experienced during a CP may lead to increased excitability in a mature network. Research in several model organisms, including mice and *Drosophila*, supports this view by showing that mature neurons are more excitable when they experience greater activity during development (Marley and Baines, 2011a; Giachello *et al.*, 2021; Styr *et al.*, 2019). Despite this progress, however, the specifics of how activity experienced during a CP influences a nervous system remains unclear. Key questions that remain unanswered include: "how does activity perturbation affect the relative contribution of excitatory and inhibitory neurons within a network?", and: "is it the extremes, or the sum of activity, experienced during a CP that is critical for mature circuit function?" It is difficult to answer these questions when conducting experiments in complex mammalian sensory networks, such as the visual and auditory networks, which have been extensively used to explore CPs (e.g., (Hooks and Chen, 2020; Nakamura *et al.*, 2020)). In this respect, the *Drosophila* larval network may provide a powerful alternative.

The larval nervous system is an experimentally-tractable and numerically simple model that is very well suited to studying CPs (Hunter *et al.*, 2021). Larvae are amenable to a range of different assays to demonstrate the impact of manipulating activity during development on a mature nervous system. For example, the electroshock assay enables assessment of 'network robustness', by measuring the ability of the nervous system to withstand or recover from strong electrical stimulation (Marley and Baines, 2011a). Similarly, functional imaging can be used to visualise locomotor network dynamics (Streit *et al.*, 2016). The *Drosophila* larval connectome project (which is near completion), has led to the mapping of individual neurons, neural circuits, and development of Gal4 lines (genetic driver lines) that enable cellular-level precision in experimental manipulation of the nervous system (reviewed in

72 (Hunter *et al.*, 2021)). It is also possible to perform electrophysiology on certain cells, such as the
73 anterior corner cell motoneuron (aCC, a.k.a MN-1b (Baines and Bate, 1998; Marley and Baines,
74 2011b)). Together, these techniques and tools can be applied to study and attempt to answer
75 questions including those posed above, by probing processes associated with an embryonic
76 locomotor CP that was first described in previous work by our group (Giachello and Baines, 2015).

77 Our earlier work showed that manipulating activity during 17-19h after egg laying (AEL), is sufficient to
78 induce significant and permanent change to locomotor network stability. It also established that the
79 range of manipulation that causes this change is broad; it extends from increased excitation during
80 this CP being sufficient to induce a seizure-like phenotype in mature larvae subjected to electroshock,
81 to a rescue of a genetic seizure mutation by reduction of network activity during the same period
82 (Giachello et al., 2015). However, the effects of activity perturbation on the specific cellular
83 components of the locomotor network have not been identified. Here, we make use of the output of
84 the connectome project to focus attention on excitatory cholinergic A18a (Hasegawa, Truman and
85 Nose, 2016) and inhibitory GABAergic A31k (Schneider-Mizell *et al.*, 2016) interneurons, as well as
86 the aCC motoneuron which these interneurons are monosynaptically connected to (Giachello *et al.*,
87 2022). Specifically, we perform patch clamp experiments on aCC to show how synaptic connectivity
88 of these single cell types (A18a or A31k) is influenced following activity perturbation during the
89 embryonic CP. We show that excessive activity during the CP permanently increases the strength of
90 the input of A18a relative to A31k, which is consistent with a significant change in the excitation:
91 inhibition (E:I) balance of the network. Next, we show that restoring E:I balance rescues the network,
92 thus providing evidence that the CP integrates the 'averaged' activity that occurs while it is open. Our
93 data suggest that 'average' activity must be balanced, so that the intrinsic properties that dictate the
94 function of the mature locomotor network are set within normal ranges.

95 **Results**

96 ***Increasing Neural Activity during Embryogenesis Permanently alters Network Function and***
97 ***Synchronicity***

98 To manipulate neural activity in developing embryos, we fed gravid (i.e. egg-laying) female flies
99 picrotoxin (PTX), which increases neural activity by non-competitive antagonism of the $GABA_A$
100 receptor (Lin *et al.*, 2012). This procedure is sufficient to expose embryos and the resulting young
101 larvae to PTX. Larval metabolism and excretion during early to mid-developmental stages removes
102 PTX, so that it is no longer detectable when assaying for effect in wall-climbing third instar larvae (L3,
103 (Marley and Baines, 2011a)). Crucially, our previous work has shown that permanent changes in
104 network function observed as a result of embryonic exposure to PTX, occur due to the change in
105 activity during the CP, which lasts from 17-19h AEL (Giachello and Baines, 2015). We measured the
106 effect of PTX-linked activity manipulation during the CP on two independent parameters at L3:
107 recovery from electroshock (which is longer in other models of CP activity manipulation (Giachello
108 and Baines, 2015)) and crawling velocity (Figure 1A-C). Embryonic exposure to PTX significantly
109 increased the duration of electroshock-induced seizures compared to controls (61.11 ± 3.94s, EtOH;

96.49 ± 6.81s, PTX; n = 36, 35; p < 0.0001) (Figure 1B). PTX exposure did not, however, influence crawling velocity (1.06 ± 0.04mm/s, EtOH; 0.98 ± 0.04mm/s, PTX; *n* = 56, 58; *p* = 0.14 (Figure 1C). This suggests that changes caused by PTX exposure during the CP were not significant enough to alter circuit function under 'normal' conditions (i.e. crawling) but clearly altered network robustness: the ability of the network to respond to strong stimulation (electroshock).

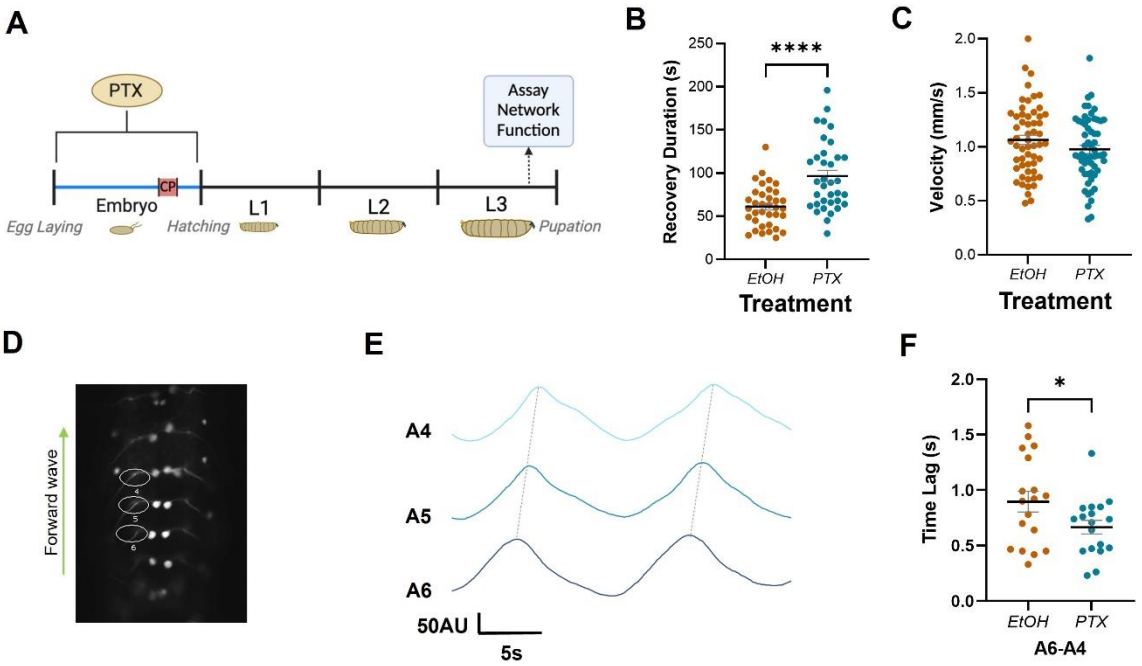

Figure 1: Increased excitation during the embryonic CP alters network stability and motoneuron network synchrony. (A) Schematic demonstrating timeline for picrotoxin (PTX) exposure, and assay of network function. PTX-induced increase in activity during development increases third-instar larval duration of recovery from induced seizure (B) but does not change crawling velocity (C). (D) ROIs captured GCaMP signal generated by forward waves passing through ipsilateral aCC motoneuron axons in the L3 ventral nerve cord, abdominal segments (A6-4). (E) Representative traces recorded in 3 adjacent abdominal segments (A6-A4), during 2 forward waves. Colours represent different segments. Synchrony was measured as the time lag (s) of activity passing between adjacent segments (i.e., between peaks, dotted lines). (F) Embryonic exposure to PTX caused a significant increase in synchronicity across segments A6-A4 versus EtOH controls.

125 With a network-level phenotype for perturbation of CP activity established (increased seizure), we
126 tested for possible correlates at the level of circuit activity within the locomotor network. In larvae,
127 normal locomotor function is characterised by stereotyped activity that is regulated by a central
128 pattern generator (CPG (Pulver *et al.*, 2015)). This pattern is formed by activity-waves that pass
129 between successive segments in the ventral nerve cord (VNC) to support peristaltic locomotion. The
130 timing (or synchronicity) of waves crossing adjacent segments is characteristic and can be measured
131 as the time lag between peaks of activity observed in adjacent aCC motoneurons. Previous work has
132 shown that synchronicity increases (i.e., time lag reduces) in the presence of mutations that
133 predispose animals to seizure (e.g. $para^{bss}$), or following acute exposure to proconvulsants (e.g. 4-
134 aminopyridine or PTX (Streit *et al.*, 2016)). We therefore quantified synchronicity of activity between
135 aCC motoneurons at L3, to investigate how embryonic exposure to PTX alters activity in the mature
136 locomotor network (Figure 1D-F).

137 Increasing neural activity during embryogenesis (PTX) significantly increased synchronicity across
138 segments A6-A4, compared to vehicle control (0.9 ± 0.09s, EtOH; 0.67 ± 0.06s, PTX; n = 18, 18; p =
139 0.05) (Figure 1F). This increased synchronicity of activity between adjacent segments is consistent
140 with, and may contribute to, the seizure phenotype observed. It likely reflects significant changes in
141 CPG properties that make it harder for larvae to recover from electroshock.

142 ***Increased Activity during the CP Alters the E:I Balance within the Locomotor Network***

143 Motoneuron activity reflects the integration of the excitatory and inhibitory premotor synaptic drive to
144 which the cell is exposed. We therefore tested the effect of embryonic exposure to PTX on the
145 synaptic drive provided by two identified premotor interneurons – one exciter and one inhibitor - which
146 are monosynaptically connected to aCC (Giachello *et al.*, 2022). Specifically, we quantified the
147 strength of cholinergic excitor A18a (a.k.a. CLI2, (Hasegawa, Truman and Nose, 2016)) and
148 GABAergic inhibitor A31k (Schneider-Mizell *et al.*, 2016) to aCC at L3, following PTX-induced activity
149 perturbation during embryonic development. To achieve this, premotor interneurons were activated
150 using optogenetics, while whole-cell patch recordings were made from aCC (Figure 2A, left-hand
151 panel).

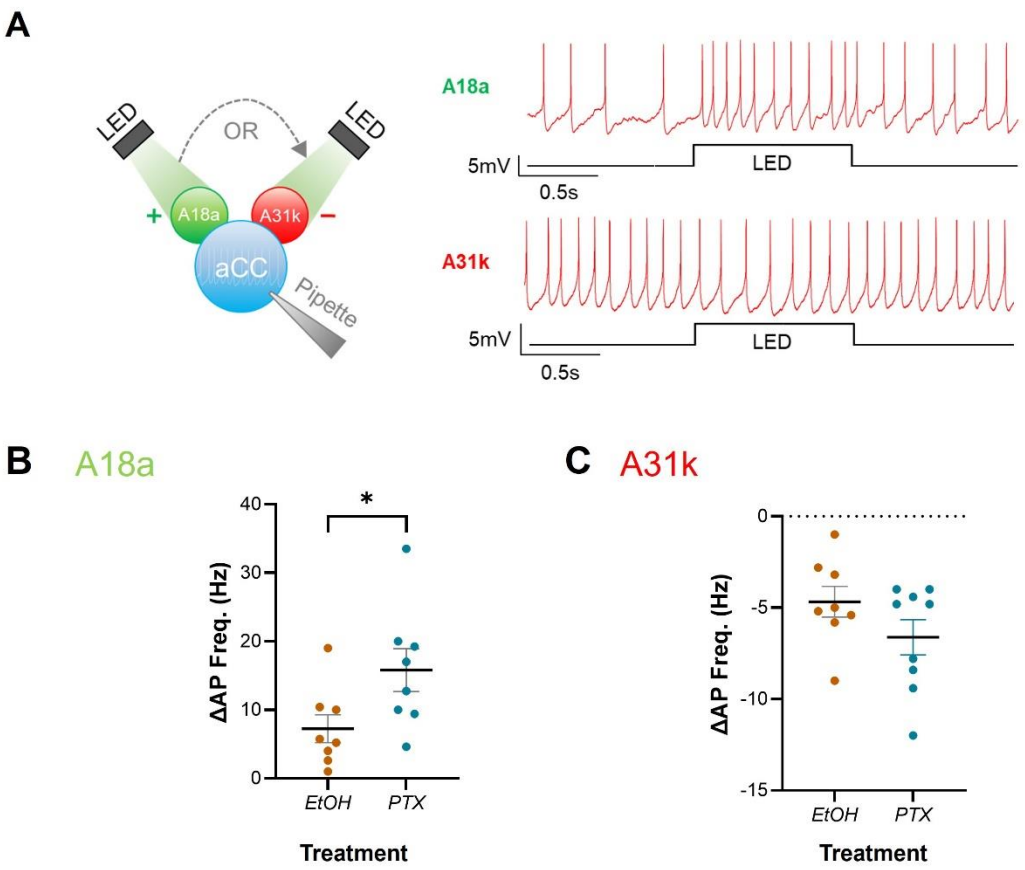

Figure 2: Increased excitation during the CP preferentially increases the strength of excitatory inputs to aCC. (A) Left-hand panel: schematic demonstrating use of optogenetics for testing strength of A18a or A31k synaptic drive on evoked action potential firing in aCC. Right-hand panel: representative traces illustrating the effect of excitatory or inhibitory input on evoked action potential firing in aCC, respectively. (B, C) current-clamp recordings wherein current (~10pA) was injected to evoke action potential firing in aCC, prior to optogenetic stimulation of premotor input. Amplitude of inputs was quantified as change in frequency of action potential firing (ΔAP Freq. (Hz)) following optogenetic stimulation of A18a or A31k. Change in action potential firing frequency in A18a, but not A31k, was significantly potentiated by embryonic exposure to PTX vs vehicle controls (EtOH).

Larval motoneurons do not generate action potentials (APs) without synaptic drive. Thus, to determine how synaptic inputs may have changed following embryonic CP manipulation, current was injected into aCC to evoke stable firing (~ 5-10Hz) before premotors were stimulated. Optogenetic activation of excitatory A18a increased AP frequency in aCC in control L3 (Figure 2A, right-hand panel) and this increase was significantly larger in L3 derived from embryos exposed to PTX (7.24 ± 2.04Hz, EtOH; 15.81 ± 3.14Hz, PTX; n = 8, 8; p = 0.04) (Figure 2B). Activation of inhibitory A31k decreased AP firing in control L3 (Figure 2A), however, this decrease was not significantly potentiated in L3 derived from embryos exposed to PTX (23.71 ± 6.76Hz, EtOH; 28.24 ± 2.4 Hz, PTX; n = 7, 7; p = 0.54) (Figure 2C). Comparing the magnitude of the changes in A18a or A31k input using an effect size calculation (see Methods for details) corroborates that excitation increased more than inhibition, as Cohen's d = 1.14 (large effect size) for A18a and 0.78 (medium effect size) for A31k. This suggests that embryonic exposure to PTX induced a shift in the E:I balance of the larval locomotor circuit to favour excitation, which is consistent with the network-level phenotypes observed (Figure 1). Thus,

our results suggest that increasing activity during the embryonic CP, increases the strength of excitatory, but not inhibitory, premotor synaptic drive.

Increased Excitatory Input to Motoneurons Reflects Increased Postsynaptic Sensitivity to Quantal Release

Increased excitatory synaptic drive to aCC may be due to either, or both, presynaptic and postsynaptic adaptations to manipulation of activity during embryogenesis. Thus, we sought to understand which of these effects may be responsible for the changes we observed. A change in the frequency of mini excitatory postsynaptic potentials (mEPSPs, a.k.a. minis) would suggest the adaptation is primarily presynaptic (e.g. increased probability of release), whilst a change in distribution and/or amplitude of minis is more consistent with a mechanism acting postsynaptically (e.g. increased or altered receptor subunits). We quantified the mean amplitude, cumulative distribution, and frequency of minis. Specifically, we began by recording spontaneous minis in wild-type larvae following embryonic exposure to PTX (Figure 3A).

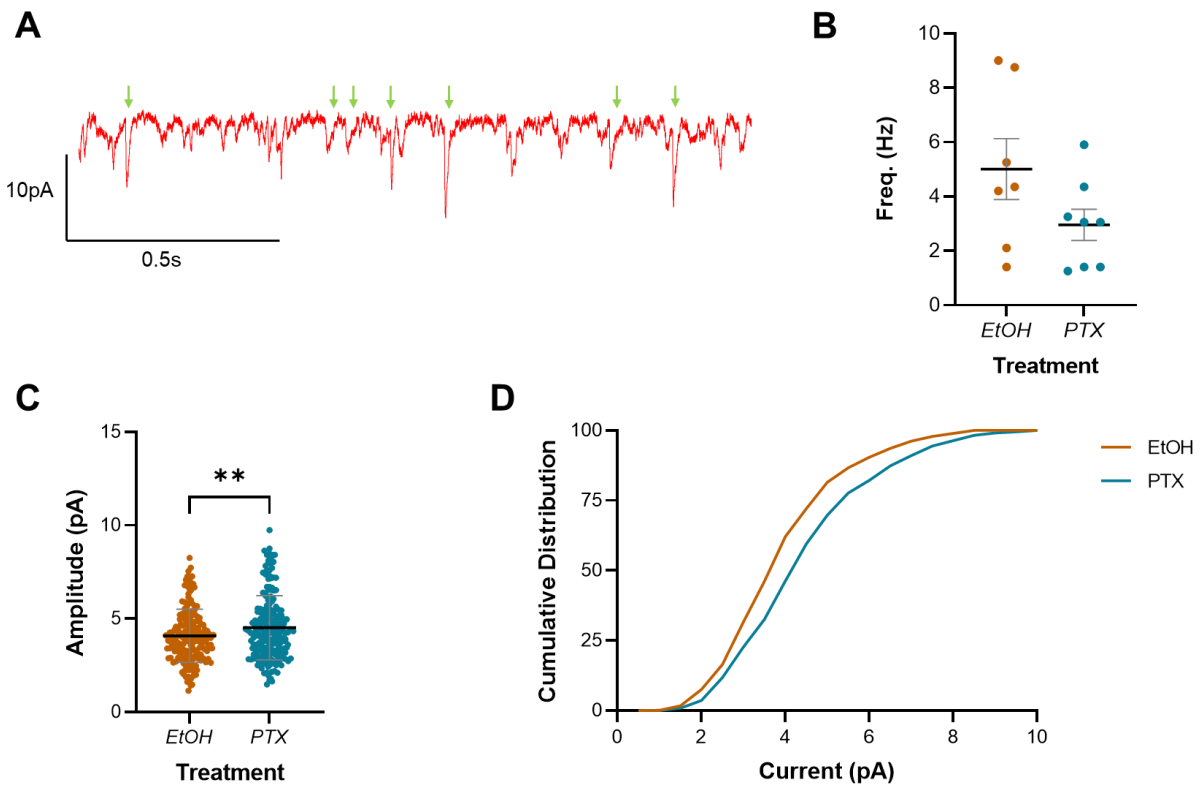

Figure 3: Increasing activity during the embryonic CP increased mini amplitude but not frequency in L3 aCC. (A) Representative trace showing minis (green arrows) in L3 aCC. (B) Mini frequency, as events observed in the first 20s of a whole-cell voltage-clamp recording (V_m held at -60mV), show no difference between vehicle controls (EtOH) and L3 exposed to picrotoxin (PTX) during embryogenesis. (C) Mini amplitude from the same recordings reveal significantly larger events in larvae that were exposed to PTX during embryogenesis, vs. vehicle controls (EtOH). (D) Cumulative distribution (%) of mini amplitude demonstrates a rightward shift in current size, following activity manipulation.

195 Whole-cell voltage-clamp recordings, made in 2μM tetrodotoxin (TTX, which limits synaptic release to
196 minis) and with V_m held at -60mV, showed that manipulating activity during embryogenesis with PTX,
197 did not change mini frequency (5.01 ± 1.12Hz, EtOH; 2.96 ± 0.57Hz, PTX; n = 7, 8; p = 0.11) (Figure
198 3B). In contrast, PTX treatment led to a significant increase in mini amplitude (4.08 ± 1.42pA, EtOH;
199 4.51 ± 1.71pA, PTX; n = 188, 199; p = 0.008) (Figure 3C), causing a corresponding rightward shift in
200 the cumulative frequency distribution (%) of currents recorded (Figure 3D). Thus, our recordings of
201 minis in aCC are consistent with a change in the postsynaptic response to excitatory quantal release.
202 However, this conclusion is based on measuring all excitatory quantal inputs to aCC, and not
203 specifically from A18a. It was, therefore, important to refine this result by restricting it to the specific
204 excitatory quantal input from this premotor interneuron.

205 It is technically challenging to record minis elicited in response to quantal release from a defined
206 neuron, because doing so requires isolating minis from a single neuron (e.g. A18a) from those
207 released by other excitatory premotors (there are many which synapse with aCC (Zarin *et al.*, 2019)).
208 To maximize our ability to do so, we adapted a technique developed in mammals, which substitutes
209 extracellular Ca^{2+} (2mM) for Sr^{2+} (8mM) (Xu-Friedman and Regehr, 1999; Bekkers and Clements,
210 1999). This substitution promotes asynchronous vesicular release (i.e., occurrence of single quantal
211 events) following firing of an evoked action potential by a presynaptic neuron, which can be recorded
212 in a postsynaptic neuron as a series of minis. Thus, we replaced Ca^{2+} (2mM) for Sr^{2+} (6mM, which
213 better supported survival of larval neurons than 8mM) and used optogenetics to stimulate A18a, while
214 recording from aCC. We validated this approach by showing that optogenetic activation of A18a, in
215 the presence of Sr^{2+}, greatly reduced evoked synaptic current but increased the frequency of minis
216 recorded in aCC (Figure S1), which is consistent with asynchronous release. Thus, under these
217 conditions, stimulation of A18a produced a series of minis predominantly released from this premotor
218 interneuron (Figure 4A).

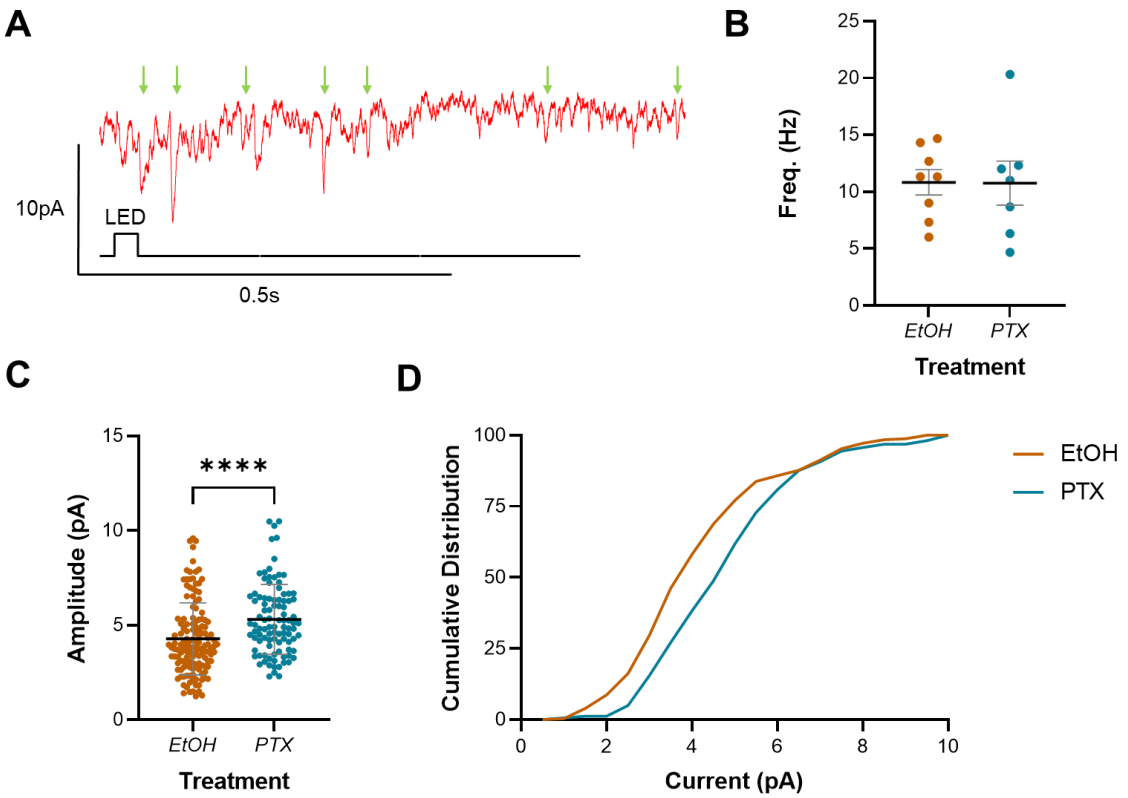

Figure 4: Increasing activity during the embryonic CP increased A18a-specific mini amplitude but not frequency in L3 aCC. (A) Representative traces showing minis (mEPSPs, green arrows) in L3 aCC (V_m held at -60mV), following optogenetic excitation of A18a. (B) Mini frequency, measured as events observed in the 3s following optogenetic stimulation of A18a (50ms light pulse) was not different between vehicle-only controls (EtOH) and L3 exposed to picrotoxin (PTX) during development. (C) Mini amplitude was significantly larger following exposure to PTX during embryogenesis, versus controls (EtOH). (D) Cumulative distribution (%) of mini amplitudes demonstrates a clear rightward shift in current size, following activity manipulation.

Analysis of whole-cell patch-clamp recordings (V_m held at -60mV) showed that there was no increase in mini frequency, in the 3s following optogenetic stimulation of A18a, in PTX versus controls (10.83 ± 1.12Hz, EtOH; 10.76 ± 1.93Hz, PTX; n = 8, 7; p = 0.97) (Figure 4B). There was, however, a significant increase in mini amplitude (4.28 ± 1.91pA, EtOH; 5.31 ± 1.85pA, PTX; n = 138, 98; p = <0.0001) (Figure 4C), and corresponding rightward shift in the cumulative distribution of current amplitudes (Figure 4D). These data are consistent with a change in the postsynaptic sensitivity of aCC to quantal release, which alters the E:I balance in the L3 locomotor circuit, following manipulation of activity during embryogenesis. Moreover, that we see the same effect in the presence of external Ca^{2+} (Figure 3) likely indicates that sensitivity to all excitatory inputs has increased.

Increased Excitation during the CP does not Alter Motoneuron Morphology or Synaptic Connectivity

Given our mini recordings suggested that the change in E:I balance may be associated with a change in the postsynaptic response to neurotransmitter release, we used high-resolution confocal microscopy to characterise the morphology and synaptic connectivity of aCC, following embryonic treatment with PTX (Figure 5).

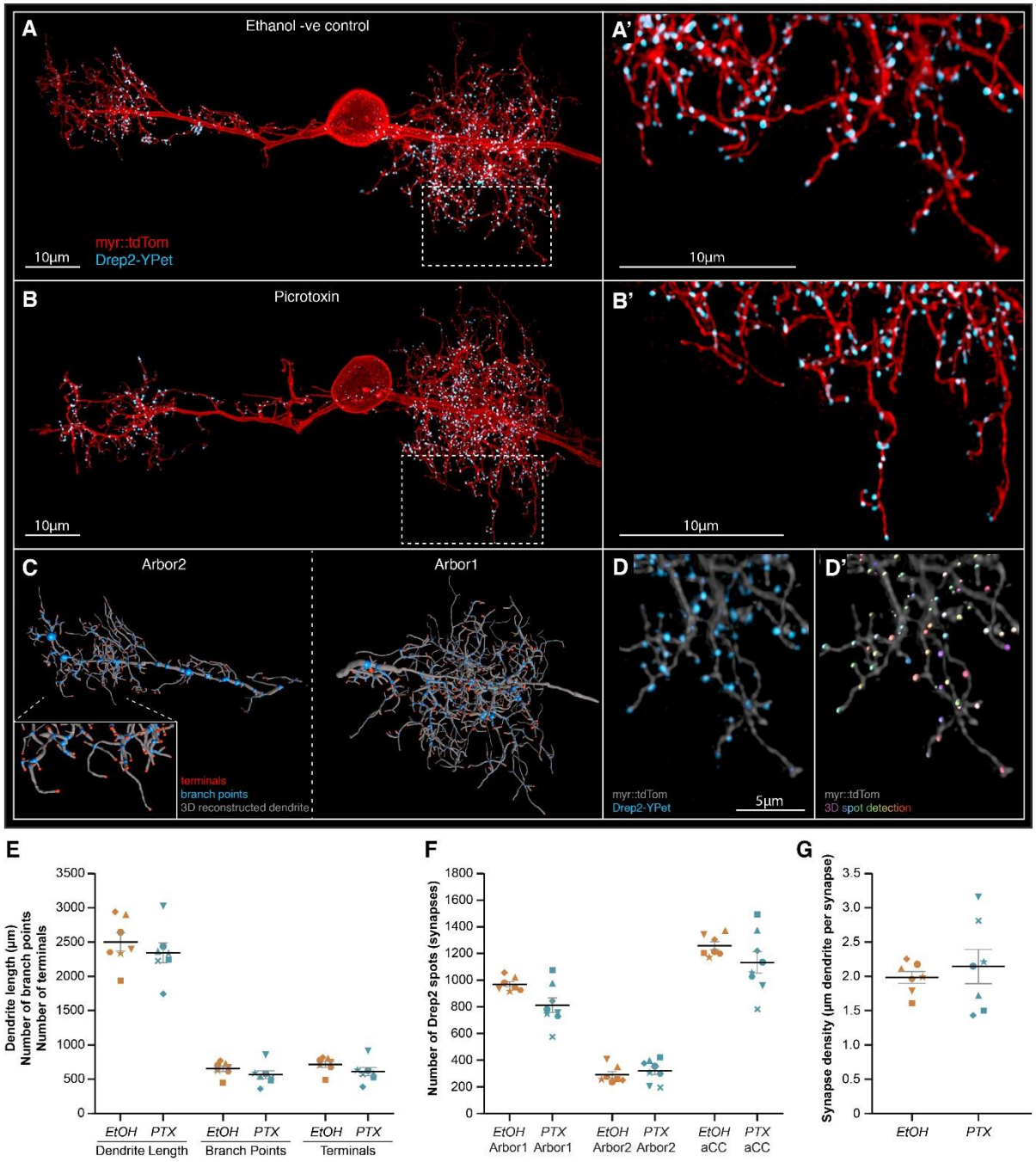

Figure 5: Increasing neural network activity by PTX exposure during development does not alter motoneuron dendritic arbor size or excitatory postsynaptic sites. (A-B) Representative images of aCC motoneurons from larval ventral nerve cords 72 hours after larval hatching (ALH), from control (A) or embryonic exposure to picrotoxin (B). aCC dendritic arbor structure is marked by membrane targeted myr::tdTomato (red), and postsynaptic excitatory sites are marked by a Drep2::YPet fusion protein (cyan). Visualisation of individual aCC motoneurons is achieved by an RN2-enhancer element driving a stochastic FLP-out LexA expression system. (C) tdTomato fluorescence was used for AI-supported 3D reconstruction of the whole aCC dendritic arbor, allowing quantification of total dendrite length (grey segments), branch points (blue spots) and terminals (red spots). (D) Following live imaging, nerve cords were fixed and stained using a fluorophore-tagged nanobody to detect the Drep2::YPet fusion protein (D), enabling high resolution and photostable imaging of Drep2::YPet puncta for quantification of excitatory postsynaptic site number by semi-automated spot detection (D'). (E) The total dendrite length, number of branch points, and number of terminals are shown, for both control and picrotoxin treatments. (F) The number of Drep2::YPet puncta for the larger ipsilateral arbor ('arbor1') the smaller contralateral arbor ('arbor2') and the combined sum across both arbors ('aCC') is shown, for both control

255 and picrotoxin treatments. (G) Synapse density, calculated as the total dendrite length divided by total Drep2::YPet positive
256 postsynaptic sites. In E-G, each point represents a single aCC cell, where the symbol shape denotes the particular cell.

257 This analysis demonstrated no obvious change in dendritic arbor length, number of branch points or
258 terminals (Figure 5E). Furthermore, the number of excitatory postsynaptic sites (Drep2 puncta
259 number) and synaptic density (μM dendrite per synapse) of aCC was unchanged following exposure
260 to PTX during embryogenesis (Figure 5F). This suggests that the changes in mini amplitude, other
261 physiology, and seizure phenotype we observed, are not due to significant change in cellular
262 morphology. Rather, it suggests the changes may be related to an alteration in excitatory postsynaptic
263 receptor number and/or sub-unit composition.

264 ***Stimulating Mechanosensory Neurons during the CP Rescues the Seizure Phenotype***
265 ***Associated with Excessive Excitatory Activity***

266 As described above, developing circuits can be exposed to various influences (light, temperature,
267 mutations etc.) which may alter levels of activity. While some of these influences will increase
268 excitation, others may decrease it. Because our data suggest that experiencing excessive excitation
269 during the CP leads to an imbalanced mature network, it is conceivable that the nervous system must
270 experience balance or a particular sum of excitatory and inhibitory influences, during the CP, to
271 encode normal network properties (Fagiolini and Hensch, 2000).

272 To test this hypothesis, we combined manipulations of predicted opposite valence to see whether, in
273 the instance that we could achieve approximately equal strengths, increased excitation and inhibition
274 would cancel each other. We chose to stimulate chordotonal (ch) neurons to counteract PTX. This is
275 because ch neurons are mechanosensitive cells that have been proposed to provide an inhibitory
276 'brake' that slows locomotor network activity during the CP (Carreira-Rosario *et al.*, 2021). We,
277 therefore, built a device to stimulate ch neurons (see Methods and Figure S2) and performed
278 experiments in which they were activated during the CP (17-19hrs AEL) or in immediately adjacent
279 periods (15-17h or 19-21h AEL) to assess the impact of the brake alone, before pairing it with PTX
280 (Figure 6A-B).

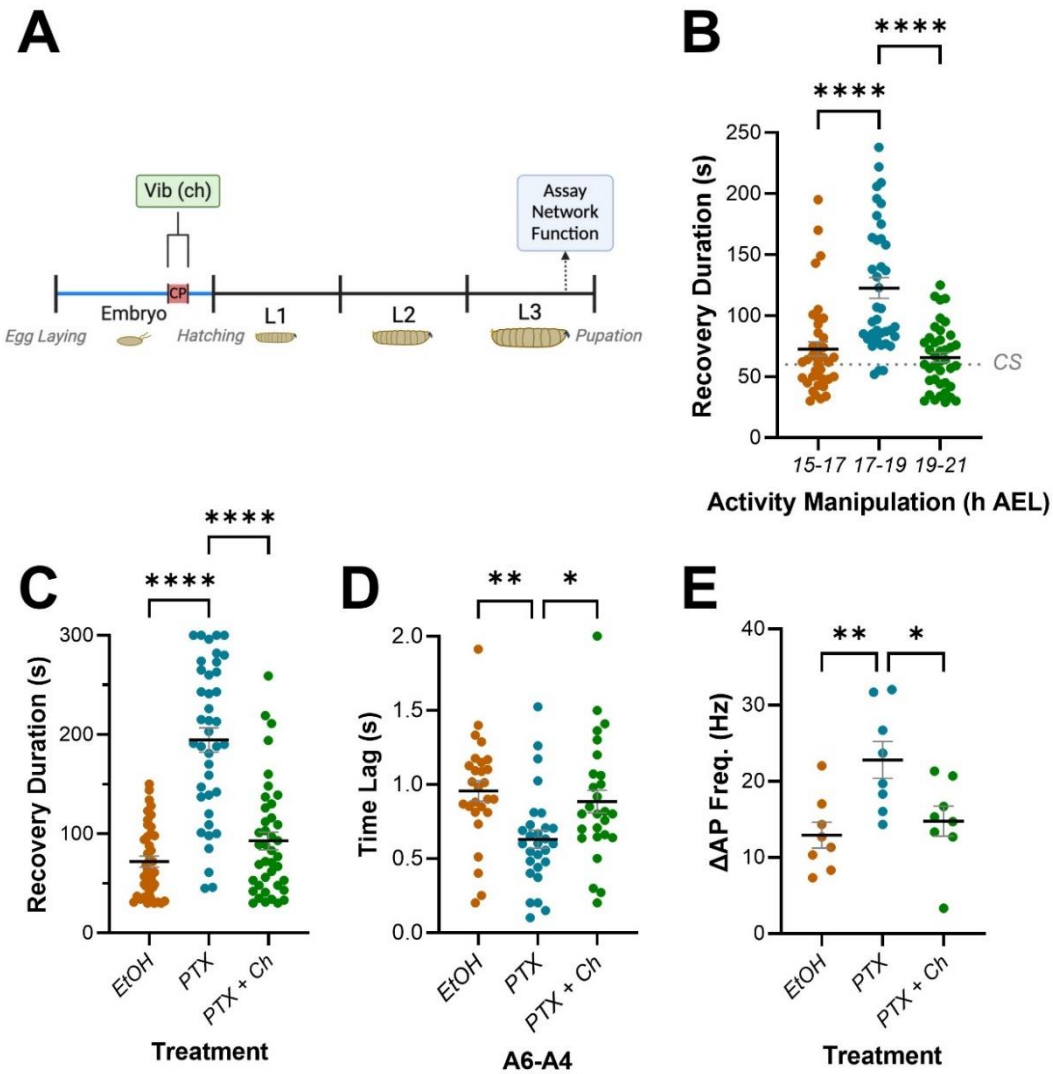

Figure 6: Activating mechanosensory neurons during the CP rescues E:I balance due to increasing activity during embryogenesis. (A) Schematic showing stimulation of mechanosensory chordotonal neurons (ch) by vibration during the CP (17-19h after egg laying, AEL). (B) Stimulating ch neurons during the CP, but not during 15-17h AEL or 19-21h AEL, significantly increases mature larval (L3) recovery duration from electroshock-induced seizure. CS is unmanipulated wild-type (*Canton-S*) controls. (C-E) Exposure to picrotoxin (PTX) during embryogenesis significantly increases mature larval (L3) recovery duration from electroshock-induced seizure, increases network synchronicity, and increases the strength of excitatory (A18a) inputs to motor neurons (aCC). All these effects are rescued by co-activation of ch neurons during the CP (PTX + Ch).

Activation of ch neurons during the CP, but not before or after it, significantly lengthened recovery from induced seizures in L3 larvae (72.69 ± 6.02s, 15-17h AEL; 122.7 ± 8.43s, 17-19h AEL; 65.83 ± 26.07s, 19-21h AEL; n = 39, 38, 40; p <0.0001 for 15-17h vs. 17-19h and 17-19h vs. 19-21h, 0.58 for 15-17h vs. 19-21h) (Figure 6B). This result shows that the majority of ch neuron activity influence on mature circuit function is, like PTX, limited to the embryonic CP. Similarly, that stimulating ch activity during the CP increases the seizure response to electroshock, is consistent with optogenetic inhibition causing the same effect (Giachello and Baines, 2015). This result also supports previous work that showed perturbing activity of sensory neurons during the locomotor CP causes lasting changes to behaviour (Fushiki, Kohsaka and Nose, 2013; Carreira-Rosario *et al.*, 2021).

298 Next, we tested how ch activity impacted the phenotypes observed for recovery from electroshock,
299 network synchronicity, and amplitude of inputs from A18a to aCC, following embryonic exposure to
300 PTX (Figure 6C-E). Remarkably, ch neuron activation provided a complete rescue of both network
301 and cellular-level phenotypes associated with embryonic exposure to PTX. Thus, recovery from
302 electroshock, which was again increased following exposure to PTX, was rescued to control levels
303 when PTX was paired with ch neuron activation (72.03 ± 5.71s, EtOH; 194.7 ± 12.22s, PTX; 92.75 ±
304 8.95s, PTX + Ch; n = 40, 40, 40; $p < 0.0001$ for EtOH vs. PTX and PTX vs. PTX vs. PTX + Ch, 0.58
305 for EtOH vs. PTX + Ch) (Figure 6C). PTX-induced increase in synchrony of activity between adjacent
306 aCC motoneurons was also rescued (0.96 ± 0.07s, EtOH; 0.63 ± 0.06s, PTX; 0.88 ± 0.08s, PTX + Ch;
307 n = 27, 28, 27; p = 0.004 for EtOH vs PTX, 0.75 for EtOH vs. PTX + Ch, 0.03 for PTX vs. PTX + Ch)
308 (Figure 6D). Finally, the increased strength of excitatory A18a inputs to aCC following exposure to
309 PTX, was rescued by stimulation of ch neurons during the CP (12.92 ± 1.704Hz, EtOH; 22.79 ±
310 2.42Hz, PTX; 14.75 ± 1.98s, PTX + Ch; n = 8, 8, 8; p = 0.008 for EtOH vs PTX, 0.53 for EtOH vs. PTX
311 + Ch, 0.023 for PTX vs. PTX + Ch) (Figure 6E). These results support the hypothesis that CPs
312 integrate the excitatory and inhibitory activity to which they are exposed, to compute a sum that leads
313 to a corresponding output in the mature locomotor network. If that sum equals balance (i.e.,
314 appropriate relative amounts of each), normal physiological function is established. An imbalance,
315 however, may lead to altered network function.

316 ***Balancing Activity during the CP Rescues Adult Behaviour caused by Genetic Mutation***

317 Next, we sought further confirmation that CPs integrate the activity they are exposed to. Specifically,
318 we tested the effect of different amplitudes of ch neuron activity (as a function of 0, 40dB, 60dB and
319 80dB speaker volume), on recovery from seizure in bang sensitive ($para^{bss}$) L3. $para^{bss}$ mutants
320 express a hypermorphic variant of the sole *Drosophila* voltage-gated sodium channel (*para*), which
321 makes neurons more excitable. Previous work has shown that excitation is increased at all stages of
322 embryonic and larval development, resulting in increased synchrony between aCC neurons and
323 increased duration of electroshock-induced seizures (Marley and Baines, 2011a; Streit *et al.*, 2016;
324 Giachello and Baines, 2015). These larvae, therefore, provided an alternative means of inducing
325 excessive excitation during the embryonic CP (rather than PTX) that we could oppose by ch neuron
326 activity, to test for impact on recovery from electroshock (Figure 7).

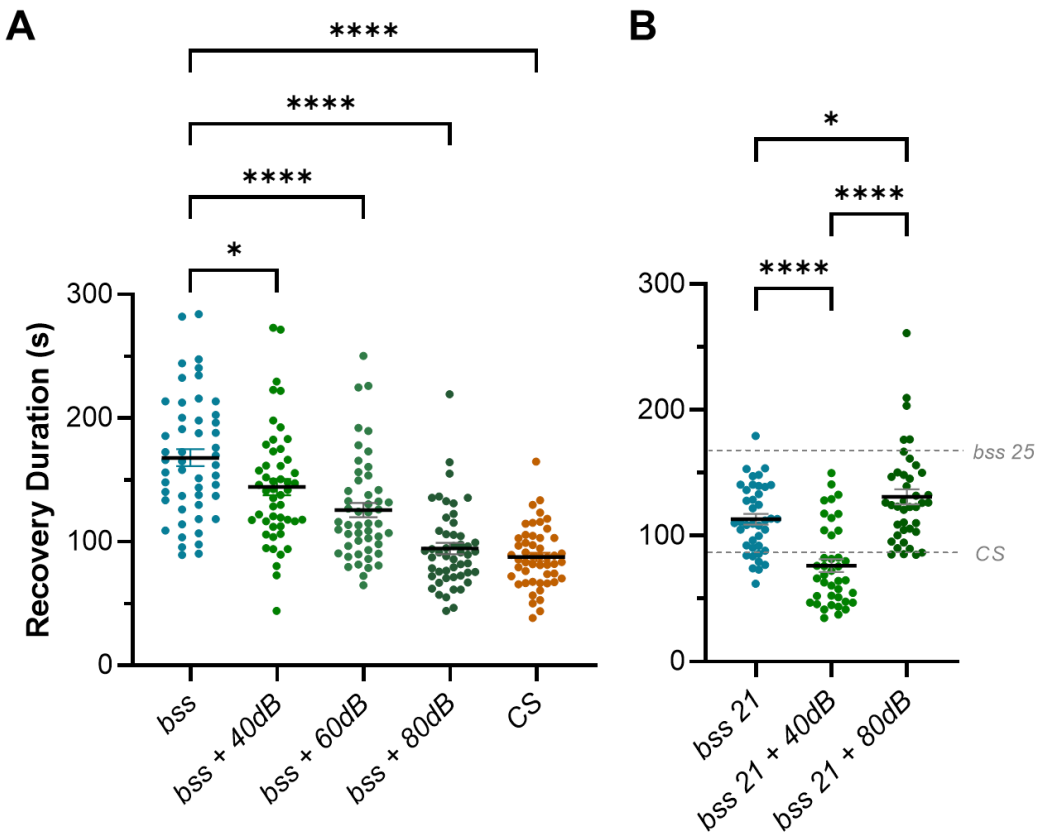

Figure 7: Restoring E:I balance during the CP rescues seizure phenotype caused by a genetic mutation. (A) The *para*^{bss} (*bss*) mutation causes lifelong neural hyperactivity, which is evident in a long duration of recovery from seizure when compared to wild-type controls (*Canton-S*). This recovery can be rescued by balancing the hyperactivity present with inhibition provided by sufficiently strong stimulation of ch neurons, during the CP (bss + 80dB). Weaker stimulation of the ch neuron-mediated inhibition provides intermediate phenotypes (bss + 60dB, bss + 40dB) that suggest the function of the mature network reflects the sum of excitatory and inhibitory activity during the CP. (B) *para*^{bss} raised at 21°C experience less excitation than those raised at 25°C (e.g. in (A)) during development, and demonstrate a reduced seizure phenotype compared to the latter. This phenotype is completely rescued by 40dB stimulation of ch neurons (vs. 80dB at 25°C (A)), which supports the idea that it is a balanced sum of excitatory and inhibitory activity during the CP, that enables normal mature network function. Similarly, exposing *para*^{bss} raised at 21°C to 80dB vibration during the CP results in a significant increase in seizure duration. We hypothesize that at this temperature, inhibition provided by ch neuron activity is greater than the increase in excitation resulting from the *para*^{bss} mutation.

In agreement with previous work (Giachello and Baines, 2015), *para*^{bss} recovery from electroshock was significantly longer than wild-type controls (168 ± 6.96s, *bss*; 87.74 ± 3.45s, *CS*; n = 50, 50; p < 0.0001). This difference was rescued completely when ch neurons were stimulated during the CP at 80dB (87.74 ± 3.45s, *CS*; 94.51 ± 4.59s, *bss* + 80dB; n = 50, 50; p = 0.91). This was the maximum strength of stimulation possible, and importantly, the effect was reduced in a dose-dependent manner as the intensity of ch stimulation during the CP decreased (125.6 ± 5.82s, *bss* + 60dB; 144.3 ± 6.61s, *bss* + 40dB; n = 50, 50; p = 0.03 for bss vs *bss* + 40dB, < 0.0001 for *bss* vs. *bss* + 60dB) (Figure 7A).

A prediction of the hypothesis that normal network function depends on a proper E:I balance during the CP, is that reduced excitation during the CP would require proportionately reduced inhibition to counteract it. To test this, we raised *para*^{bss} at 21°C, which reduces the duration of evoked seizure

350 when compared to animals raised at 25°C (168 ± 6.96s, *bss 25*; 113.2 ± 4.28s, *bss 21*; n = 40, 50; p <
351 0.0001). This is presumably due to reduced levels of excitation at this developmental temperature. At
352 21°C, stimulating ch activity during the CP using 40dB is sufficient to completely suppress seizure
353 behaviour (76.24 ± 5.07s, *bss 21 + 40dB*; 86.68 ± 4.2s, *CS*; n = 40, 40; p < 0.44). Notably, ch activity
354 at 80dB induces a seizure phenotype (130.8 ± 5.6s, *bss 21 + 80dB*; 86.68 ± 4.2s, *CS*; n = 40, 40; p <
355 0.0001), which is consistent with 80dB ch-induced inhibition outweighing $para^{bss}$-induced excitation at
356 21°C (Figure 7B). Combined, these results support the hypothesis that the CP integrates the
357 excitatory and inhibitory activity to which the locomotor network is exposed, using the sum (relative
358 balance, or E:I) to set key network parameters that are then 'locked in' to the mature locomotor
359 network. Proper balance leads to normal function, while imbalance may cause dysfunction.

360 **Discussion**

361 A large body of work, mostly performed in rodents, has shown that maturation of neural circuits is
362 dependent on an interplay between excitatory and inhibitory activity, particularly during developmental
363 CPs (Wong-Riley, 2021; Hensch, 2005; Hensch and Bilimoria, 2012; Gervain *et al.*, 2013). CPs often
364 reflect a change from spontaneous to patterned activity within neural networks (Coulson *et al.*, 2022).
365 Early spontaneous activity that occurs prior to CP opening, is predominantly excitatory, and notably
366 includes excitatory GABAergic signalling (Ben-Ari, 2002). Thus, the E:I balance is strongly biased
367 towards excitation prior to the opening of a CP (Allene *et al.*, 2008). This early developmental phase
368 seemingly facilitates the development of neuronal electrical properties and synaptic connectivity
369 (Baines and Pym, 2006). However, as sensory input becomes active, inhibitory signalling increases
370 (with GABA now assuming its mature inhibitory signalling mode). This coincides with, and may
371 enable, CP opening (Hensch, 2005; Hensch and Bilimoria, 2012).

372 Key outstanding questions related to CPs are: which network properties are set whilst a CP is open?
373 And are these properties, which are often 'locked in', deterministic for the trajectory of a developing
374 network? Our work provides further evidence that appropriate E:I during a CP is necessary for normal
375 function in mature neural networks, which supports previous work (Giachello and Baines, 2015).
376 Importantly, however, our work also presents novel insight into the precise role that appropriate E:I
377 balance contributes during CPs, at a level of synaptic detail that is difficult to attain in other models.
378 We achieved this insight by exploiting the genetic tractability (courtesy of tools developed as a
379 consequence of the *Drosophila* connectome project (Ohyama *et al.*, 2015; Zheng *et al.*, 2018;
380 Scheffer *et al.*, 2020)) and accessibility of the larval nervous system (reviewed in Hunter et al., 2021),
381 to demonstrate that increasing activity during the CP alters mature network E:I to affect permanent
382 change to locomotor network function.

383 Collectively, our results show that activity manipulation during a CP alters the E:I balance in defined
384 components of the larval locomotor circuit. Specifically, we observe that the strength of input from an
385 excitor (cholinergic A18a) to a motoneuron (aCC), increased more than the input from an inhibitor
386 (GABAergic A31k). We identified an increase in the amplitude of minis, which suggests the primary
387 mechanism that alters excitability is postsynaptic. Similar changes to synaptic physiology have been

388 reported in mammalian systems. For example, monocular deprivation in rat increases excitability in
389 layer 4 of the visual cortex, skewing the E:I balance towards excitation (Maffei, Nelson and Turrigiano,
390 2004). However, the complexity of the visual system obscures definitive conclusions because of
391 apparent confounding observations of increasing inhibition in different components of the same
392 circuitry (Maffei, Nelson and Turrigiano, 2004). Interestingly, these observations mirror our results
393 where we report increases in both excitation and inhibition, but show that the former predominates,
394 thus altering E:I balance. Moreover, and again similar to our findings, monocular deprivation in rats is
395 sufficient to increase mini amplitude indicative of active postsynaptic mechanisms for altered
396 excitability. Specifically, mini amplitude first declines following monocular deprivation, but after 3-6
397 days is potentiated due to homeostatic synaptic scaling (Lambo and Turrigiano, 2013). This
398 observation suggests that homeostatic compensation can alter properties set during a CP and thus
399 the final effect to any given network is likely to be due to a mix of CP-dependent and homeostatic-
400 dependent change. The ability to record from identified network components and capability to explore
401 along the entire developmental timeline of the *Drosophila* larval locomotor circuit, offers the prospect
402 of exploring this in greater detail. For example, it remains unknown if the effects we observe in late L3
403 are a result of only CP-related mechanisms, or are a consequence of the former, plus additional
404 homeostatic compensation occurring during larval life. The ability to record from *Drosophila* embryos
405 (Baines and Bate, 1998), in addition to all larval stages, means that this important question can be
406 addressed experimentally.

407 Our results that show excitatory input to motoneurons is increased to a greater extent than inhibitory
408 input, when the developing circuit is exposed to excessive activity during the CP, could be considered
409 surprising. It may be assumed that the nervous system should compensate for increased excitation,
410 by decreasing excitability through either: (1) reducing excitatory (A18a) input strength; (2) increasing
411 inhibitory (A31k) input strength; (3) both 1 and 2. A potential explanation may be that activity during a
412 CP is not compensated for; rather, it is used to encode homeostatic set points to which the mature
413 nervous system will continually attempt to return. Set points are defined as 'ranges of activity'
414 associated with normal circuit function, so that activity outside of the set point may induce abnormal
415 behaviour (Styr *et al.*, 2019; Truszkowski and Aizenman, 2015; Tien and Kerschensteiner, 2018).
416 Inappropriate E:I balance during the CP may establish a non-physiologically relevant set point, which
417 then serves as the basis for homeostasis once the CP is closed. If CPs capture, rather than
418 compensate for activity to establish set points, it is logical that the strength of premotor inputs
419 increases in accordance with the hyperexcitability induced by exposure to PTX during the CP. It may
420 also explain how the otherwise life-long hyperexcitation caused by the $para^{bss}$ mutation, can be
421 rescued by inhibiting neural activity during the short 2h CP window (Giachello and Baines, 2015).

422 Our observations of lasting change to synaptic physiology provides further evidence to support the
423 hypothesis that physiologically-balanced E:I, during a CP, is key to normal network function. Similarly,
424 our results that show that a ch neuron inhibitory "brake" (Carreira-Rosario *et al.*, 2021) provides a
425 dose-dependent rescue of excessive excitation caused by PTX or the $para^{bss}$ mutation, are
426 consistent with a CP integrating activity to which it is exposed. It is notable that 80db-induced ch

427 activity rescued both the PTX and *para*^{bss} seizure phenotype completely. The simplest explanation for
428 this that 80dB inhibition matches the strength of both types of increased excitation, so they cancel
429 each other out. That is to say, the degree of hyperexcitation caused by PTX and *para*^{bss} are similar.
430 However, this may be an overly simplistic assumption, and instead ch neuron activity may achieve
431 rescue via alternate means, including, but not limited to, an influence on activity-dependent CPG
432 wave frequency during the CP.

433 Ch neurons have been implicated in establishing CPG rhythm via connections to premotor and
434 pacemaker neurons A27h and M, respectively (Zeng *et al.*, 2021). This rhythm-setting function may
435 be related to relaying early muscle activity and coordinating it with the output of the CNS. Muscles
436 produce myogenic activity and twitch early in development, beginning around 15hrs AEL (Crisp *et al.*,
437 2008; Crisp, Evers and Bate, 2011; Baines and Bate, 1998). Given that this is just before the
438 locomotor circuit CP (17-19 h AEL) (Giachello and Baines, 2015), it is possible that the development
439 of coordinated activity in the locomotor circuit depends on a succession of set points established in
440 muscles, then peripheral neurons (e.g. ch neurons), central neurons (A18a, A31k, M and A27h
441 neurons) and motor neurons (aCC). Finally, despite the ch brake being inhibitory in the sense that it
442 slows the CPG (Carreira-Rosario *et al.*, 2021) and counteracts the excessive excitation provided by
443 PTX or *para*^{bss}, electrophysiological recording from aCC shows that stimulating ch neurons (by
444 optogenetics), is sufficient to depolarise aCC (IH & RAB, unpublished data). The idea that a
445 depolarising input can inhibit activity in the locomotor circuit is likely explained by the contribution ch
446 neurons make to the CPG rhythm. CPG activity causes regular, significant depolarisation of aCC in
447 the form of spontaneous rhythmic currents (SRCs). SRCs may be followed by refractory periods that
448 prevent further (i.e. greater) activity occurring in the network. This could be explored in future work.

449 The rescue of increased seizure in *para*^{bss} reported in Giachello et al., 2015, was achieved using a
450 different modality to inhibit neurons (optogenetics), than we have used here (vibration). The latter is
451 more physiological, as it is known that mechanoreceptors provide activity that contributes to normal
452 development of locomotor circuits / CPGs in flies and other animals (Carreira-Rosario *et al.*, 2021;
453 Zeng *et al.*, 2021). Indeed, our validation experiment showed that activating proprioceptors during just
454 the CP, in the absence of PTX, is sufficient to induce a seizure phenotype. This is reminiscent of other
455 work that implies abnormal proprioceptive activity during development can contribute to neurological
456 disorders such as developmental coordination disorder (DCD, (Tran *et al.*, 2022)). Thus, our protocol
457 for inducing activity in ch mechanosensory neurons may be used as a model for further investigation
458 of DCD and related conditions.

459 Vibration represents one of a growing list of approaches that show that manipulating neural activity
460 during development can cause permanent change to network function. Other methods for
461 manipulating activity include endogenous mutations (e.g. *para*^{bss}), exposure to drugs (PTX or
462 phenytoin (Giachello and Baines, 2015)), genetically targeted expression of tetanus toxin (Carreira-
463 Rosario *et al.*, 2021), temperature (Kiral *et al.*, 2021) and light (via optogenetics (Giachello and
464 Baines, 2015)). Some (e.g., temperature and vibration) may be encountered by animals developing in
465 the wild, and can be excitatory or inhibitory (for example, altered temperature can increase or

466 decrease neural activity during development). Thus, our work, in combination with that conducted by
467 others, suggests that CPs may 'measure' neural activity, which is influenced by various environmental
468 and internal factors. This measurement is used to set key network parameters according to the
469 context in which the circuit functions. In support of this, a recent study reports that synaptic number in
470 the *Drosophila* adult eye scales inversely with developmental temperature (Kiral *et al.*, 2021).
471 Behavioural analysis indicates that this phenomenon ensures that adult movement is highly
472 dependent on, and optimized for, developmental temperature.

473 In conclusion, our work provides novel insight into how activity manipulation during a defined CP,
474 results in mature network change. Specifically, we show a clear and lasting change to network E:I
475 balance that leaves the locomotor network prone to seizure following a sufficiently large stimulus, and
476 relate this to cellular and synaptic-level changes in the circuit. The changes we observed may reflect
477 a network that has encoded a non-physiological set point that, though capable of supporting normal
478 locomotion, is not sufficient to guard against the effects of strong stimulation. Finally, we show that
479 changes induced by excessive excitation can be compensated by inhibition provided by
480 mechanosensory neurons, in a dose-dependent manner. This supports the view that a CP acts to
481 tune a developing network based on the influences on activity, to which it is exposed.

482 **Materials and Methods**

483 *Drosophila Rearing and Stocks:*

484 *Drosophila* stocks were kept on standard corn meal medium, at 25˚C. For all experiments where
485 crosses were necessary, stocks were selected and combined as a 1:2 ratio of Gal4-line males to
486 UAS-line virgin females.

487 Wild-type *Canton-S* or bang-sensitive (*para*^{bss1}) were from our lab stocks. The following lines were
488 used for GCaMP imaging and/ or electrophysiology: *w;;GMR94G06-Gal4* (aCC, gift from Matthias
489 Landgraf); *w-; 15B07-Gal4* (A18a, gift from Aref Zarin); *R20A03-p65ADzp in attP40; R93B07-*
490 *ZpGDBD in attP2* (A31k, gift from Akinao Nose); *iav[3621]/C(1)DX, y[1] f[1]* (chordotonal neurons,
491 BDSC #52273); *w[*]; P{y[+t7.7] w[+mC]=20XUAS-Chronos::mVenus}attP40* (BDSC #77115);
492 *w[1118]; P{y[+t7.7] w[+mC]=20XUAS-IVS-jGCaMP7f}su(Hw)attP5* (BDSC #80906); *w-; 13xLexAop2-*
493 *Flp2@attP40, Drep2*^{FonYPet}*, 13xLexAop2-IVS-myr::tdTom @ su(HW)attP5/CyO, Dfd-GMR::YFP;*
494 *RN2-FLP-hopA, tub-FRT-stop-FRT-LexAVP16 (No.5)/TM6b, Sb, Dfd-GMR::YFP* (a.k.a. RN2-FLP
495 LexA-tdTom Drep2::YPet) for microscopy.

496 *Manipulation of Activity during Development:*

497 *PTX feeding protocol for increasing neural activity during development:* PTX and vehicle food were
498 made by pipetting 20µl 25mg/ ml PTX, or an equivalent volume of vehicle (ethanol, EtOH) to 1ml of
499 ddH_2O, for a final concentration of 415µm PTX. 4g yeast extract powder (Melford, UK) was stirred into
500 the 1ml ddH_2O to make 5g yeast paste food. ~1ml of either PTX or control food was then placed on
501 the surface of a 6ml grape agar plate. Flies were added to a 50ml beaker using a funnel, and the

502 beaker was connected to a grape agar plate (with food) using a pressure-fit plastic collar, to form a
503 small laying pot. Laying pots were left at 18˚C for 48h (over weekend) to allow flies to acclimate and
504 eat the food. After 48h, pots were moved to 25˚C and changed (beaker swapped and food
505 replenished) at 10:00 and 15:00 every day, for five days (Monday-Friday). Embryos were collected
506 from the surface of grape agar plates, using a wet paintbrush, for the final three days (Wednesday-
507 Friday) of this process. Following collection, embryos (of either sex) were gently placed on the surface
508 of vials containing either: (1) corn meal medium enriched with ~70µM all-trans retinal (Sigma-Aldrich,
509 UK, 50µl of 100mM stock pipetted onto ~7ml food and left to dry before embryos were added), a
510 cofactor chromophore necessary for activation of channelrhodopsin, for animals to be used in
511 optogenetic experiments; (2) normal corn meal medium, in the case of embryos developing into
512 larvae used in GCaMP imaging or behavioural experiments.

513 *Vibration protocol for activating chordotonal neurons during embryonic development:*

514 Gravid females were fed either: (1) normal corn meal medium where effect of chordotonal neurons
515 was not used to rescue effect of PTX (e.g. *Canton-S* and *para*^{bss} experiments); (2) 830µm PTX food
516 (as above), when chordotonal neuron activity was used to rescue effect of PTX. Male and female
517 embryos were collected Monday-Thursday and timed precisely (from animals laying in a four-hour
518 window between 10:30-14:30), to ensure that the developmental stage at which embryos were
519 exposed to vibration included the 17-19h after egg laying (AEL) CP. Embryos were collected onto
520 grape agar plates and arranged dorsal side up. Plates were then placed on a custom-made perspex
521 shelf glued to a speaker (Adafruit STEMMA Speaker - Plug and Play Audio Amplifier), in a 25°C
522 incubator. The speaker was wired to an Arduino Uno Rev 3 printed circuit board with an ATmega328P
523 microcontroller, that was programmed using C^{++}, via the Arduino IDE (Arduino 1.8.19), using the
524 following code: https://github.com/virhunter/vibrationduringdevelopment/blob/main/timedbuzzer.

525 The code was written and refined by several users of the Arduino forum. The original forum thread,
526 which includes the usernames of those who contributed to it, is visible at:
527 https://forum.arduino.cc/t/help-with-basic-buzzer-tone-program-will-acknowledge-in-scientific-journal-
528 article-in-return/1027170/25. The code instructed the Arduino to power the speakers to provide a
529 1kHz tone (vibration) to the perspex shelf (so the embryos), with an on-off frequency of 0.5Hz (ON 1s,
530 OFF 1s) for 6 hours, starting 12.75h after a button was pressed. Thus, once embryos were collected
531 and placed on the shelf at 14:30, the button was pressed at 14:45, and stimulation was delivered to
532 embryos between 03:30 and 09:30. Tone volume was 80dB for all experiments besides those where
533 others are stated explicitly (e.g., 40 and 60dB).

534 *Crawling velocity:*

535 Male and female wall-climbing third instar larvae (L3) were selected from vials and washed to remove
536 food residue. They were dried with a tissue and placed in the centre of a 1% agarose gel arena
537 surrounded by a 5M NaCl (Sigma-Aldrich) moat. Animals were then left to acclimatise to the arena
538 and recover from handling, for 30 seconds. Crawling was then recorded for 120s, using a DanioVision
539 observation chamber (Noldus, Netherlands). Only larvae that spent 100% of recording time within the

540 gel arena were included in analysis (the few that entered the moat, were excluded). Velocity was
541 calculated from movement of a centroid automatically identified by the tracking system, in mm/s, by
542 the Ethovision software (Noldus, v. XT 11).

543 *Recovery from electroshock*:

544 Assays were conducted as described previously (Marley and Baines, 2011a). In brief, male and
545 female wall-climbing L3 larvae were selected from vials and washed to remove food residue. L3 were
546 dried with a tissue and placed on an plastic plate lid to recover from handling. Once animals had
547 recovered and normal crawling had resumed, a handheld stimulator composed of two tungsten wires
548 fixed to a nonconducting rod (tips of the two wires (0.1 mm diameter) were set ~1–2 mm apart) was
549 positioned and very gently pressed into the larval cuticle, perpendicular to and over the approximate
550 position of the CNS. A direct current pulse (10V, 1s) generated by a DS2A Mk.II stimulator (Digitimer
551 Ltd., UK) was delivered via the probe to the animals, which usually responded with a sustained
552 contraction and subsequent immobility representing seizure-like behaviour. The time to resumption of
553 normal behaviour (regular, whole body peristaltic waves that produce forward locomotion) was
554 recorded and defined as duration of recovery from seizure.

555 *Electrophysiology:*

556 Recordings were performed as described previously (Baines et al., 1990; Marley and Baines, 2011),
557 in male and female L3 larvae. In brief, the protocol was as follows: larvae were dissected in a dish in
558 saline (135mM NaCl (Fisher Scientific, UK), 5mM KCl (Fisher Scientific), 4mM $MgCl_2 \cdot 6H_2O$ (Sigma-
559 Aldrich), 2mM $CaCl_2 \cdot 2H_2O$ (Fisher Scientific), 5mM TES (Sigma-Aldrich), 36mM sucrose (Fisher
560 Scientific), at pH 7.15) to remove the CNS. The isolated CNS preparation was then transferred to a
561 200µl droplet of external saline, within which it was laid flat (dorsal side up) and glued to a Sylgard-
562 coated cover slip on a slide. 200µM mecamylamine (Sigma-Aldrich) was added to the droplet of saline
563 for recordings made following optogenetic activation of A31k, but was not added for those made
564 following activation of cholinergic A18a.

565 Before recording, interneuron Gal4 and mVenus-tagged reporter line expression (e.g. 15B07-Gal4 x
566 UAS-Chronos::mVenus) was checked by momentarily exposing preparations to blue light (470nm
567 OptoLED, Cairn Instruments, UK), while viewing them under a microscope (model BX51WI, Olympus,
568 UK). Once expression was confirmed, aCC motoneurons present in the VNC segments that
569 expressed the interneuron Gal4 and reporter, were identified using bright-field microscopy. 1%
570 protease (Sigma-Aldrich) was applied to those segments to remove overlaying glia, to facilitate
571 access to aCC. Recordings were made using borosilicate glass pipettes (GC100F-10, Harvard
572 Apparatus, USA) that were fire polished to resistances of 10–15MΩ and filled with intracellular saline
573 (140 mM K1-D-gluconate (Sigma-Aldrich), 2 mM MgCl2 · 6H2O (Sigma-Aldrich), 2 mM EGTA (Sigma-
574 Aldrich), 5 mM KCl (Fisher Scientific), and 20 mM HEPES (Sigma-Aldrich), at pH 7.4). Input
575 resistance was measured in the 'whole cell' conformation, and only cells that: (1) had an input
576 resistance ≥0.5GΩ; (2) had a membrane potential ≤–40 mV; (3) were not firing action potentials at
577 rest, were used for experiments. Data was captured using a Multiclamp 700B amplifier controlled by

578 pCLAMP (v. 11.2.1), via a analog-to-digital converter (model Digidata 1440A, Molecular Devices, CA,
579 USA). Traces were sampled at 20 kHz and filtered online at 10 kHz.

580 Current-clamp recordings from aCC were made by injecting current (~5-10 pA) sufficient to evoke
581 action potentials (APs) in aCC, at a frequency of ~5–10 Hz. Premotor synaptic drive was elicited by
582 optogenetic stimulation of interneurons using green light (565nm OptoLED, Cairn Instruments)
583 controlled by a Clampex (version 10.7) protocol comprised of three sweeps (repetitions) of 1s LED off,
584 1s on, 1s off, for each preparation. Change in frequency (ΔAP Freq. (Hz)) was calculated as the
585 difference in number of action potentials firing before and during optogenetic stimulation.

586 *GCaMP Imaging:*

587 Imaging was performed on aCC motor neurons in w; UAS-GCamP7f x w;;GMR94GO-Gal4 male and
588 female L3 derived from gravid females fed PTX, or vehicle control (see *Manipulation of Activity during*
589 *Development*). larvae were dissected in a dish in external saline (see *Electrophysiology*) to remove
590 the CNS. The isolated CNS preparation was then transferred to a droplet of saline, within which it was
591 laid flat (dorsal side up) on a Sylgard-coated cover slip on a slide. The slide was positioned under a
592 microscope (model BX51WI, Olympus) with a Hamamatsu ORCA-flash 4.0 C114440 digital camera,
593 and the CNS viewed using a x20 water immersion lens. Blue light (a 470nm OptoLED, Cairn
594 Instruments) was used to excite GCaMP, and fluoresence was recorded for 180s at a 10Hz imaging
595 rate, using Winflour v4.1.3 (University of Strathclyde). During analysis, ROIs were placed on aCC
596 axons, on the same side of the VNC, from A6-A4, and exported into Clampex (10.7). Traces were
597 smoothed (add type and amount), with forward wave propagation being measured between adjacent
598 ipsilateral ROI's. Time lag was measured as the mean duration between events (peak amplitudes),
599 between segments A6-A5 and A5-A4. Means were calculated from up to 5 individual measures of
600 time lag.

601 *Confocal Microscopy:*

602 *PTX feeding protocol:* Picrotoxin (Merck, NJ, USA) was prepared to 25mg/ ml in 100% ethanol, then
603 40ul of this stock diluted 50-fold by adding to 1960ul ddH_2O then mixed with 8g of yeast extract powder
604 (Melford), while for controls the equivalent amount of EtOH only was used. Canton-S virgin females
605 were crossed to RN2-FLP LexA-tdTom Drep2::YPet males (see above for complete genotype) and left
606 to mate in vials at 25°C for 24 hours. Mated flies were distributed to two laying pots with apple juice
607 agar plates, with an excess (~0.5g) of either picrotoxin or control yeast extract paste. Laying pots were
608 kept at 25°C, yeast plates changed and discarded daily for three days to ensure sufficient time for drug
609 exposure. Thereafter, newly hatched larvae aged to within 1 hour of one another were picked from
610 laying plates and transferred to new apple juice agar plates with an excess of normal yeast paste (dried
611 baker's yeast and ddH_2O), and allowed to develop at 25°C for 72 hours.

612 *Imaging:* At 72 hours after larval hatching (ALH), larvae of the correct genotype were chosen by
613 selection against the Dfd-GMR-YFP balancer. Larval nerve cords were dissected at room temperature
614 in Sorensen's saline, adhered to a poly-L-lysine (Merck) coated coverglass, and imaged 'live' within a
615 drop of Sorensen's saline on a Leica Stellaris 5 upright confocal microscope with a Leica 506148 HC

616 APO L 63x/0.9 W U-V-I Water Immersion objective. The following imaging settings were used: format
617 800x800, 16bit, scan speed 400Hz, bidirectional scanning, pinhole 1 Airy Unit, z step size 0.3um,
618 sequential frame scanning. For Drep2::YFP detection: excitation 514nm at 1.5% power, gain 20,
619 emission collection window 520-540nm, frame accumulation 3. For myr::tdTom detection: excitation
620 561nm at 2% power, gain 15, emission collection window 570-700nm, line accumulation 4. Inbuilt Leica
621 LIGHTNING deconvolution software was used, with default settings optimised for water immersion.
622 Following acquisition of the 'live' image, nerve cords were fixed for 15 minutes at room temperature in
623 2% PFA in Sorensen's saline, washed 3x in Sorensen's saline, blocked for 1 hour at 4°C in blocking
624 solution (1x Sorensen's saline, 0.3% Triton-X-100, 0.25% BSA) and then incubated for 15 hours at 4°C
625 with FluoTag-X4 anti-RFP STAR635P and FluoTag-X4 anti-GFP ATTO488 (NanoTag
626 Biotechnologies), both diluted 1:500 in blocking solution. Stained samples were then washed 3x in
627 Sorensen's saline at 4°C for >1 hour, before imaging again. Imaging settings for nanobody-stained
628 samples were the same as for live samples, with the following specific differences: format 1024x1024,
629 z step size 0.25um. For Drep2::YFP > anti-GFP ATTO488 detection: excitation 488nm at 1.5% power,
630 gain 2.5, emission collection window 498-580nm, line averaging 3, line accumulation 3. For myr::tdTom
631 > anti-RFP STAR635P detection: excitation 638nm at 2% power, gain 15, emission collection window
632 648-830nm, line averaging 3, line accumulation 3.

633 *Image analysis:* Imaris v10.0 software (Bitplane) was used for image analysis. Dendrites were
634 reconstructed from the myr::tdTom channel of 'live images' as dendrite morphology is clearer pre-
635 fixation. The Imaris filaments module was used for dendrite reconstruction, using the tree autopath
636 algorithm, with the starting points threshold set to include just one starting point on the cell body. Seed
637 points for segments multiscale points were set to a thinnest diameter of 0.01um, and largest diameter
638 of 3um. Iterative rounds of user-informed AI training were used for seed point classification until all seed
639 points correctly coincided with dendrites, followed by iterative rounds of AI training for segment
640 classification. A tree-build maximum gap length of 5um was used. Drep2::YPet marking post-synaptic
641 sites was detected from the fixed and nanobody stained images, since Drep2::YPet>anti-GFP
642 ATTO488 showed good photostability through the z-stack compared with 'live' YPet protein, which
643 suffered substantial photobleaching through the course of acquiring a 'live' image stack. The Imaris
644 spots module was used for Drep2::YPet spot detection, using an estimated xy diameter of 0.1um, and
645 z diameter of 0.5um. The spot quality threshold was informed by the frequency histogram and set to
646 the trough point, at which any further decrease in threshold results in a sharp increase in spot number,
647 corresponding to false positive spots detected outside the cell from low-level background. In this way,
648 all Drep2::YPet puncta of different sizes were detected, while avoiding false positives from low level
649 background.

650

Statistical Analysis:

Data were imported into and organised in Microsoft Excel (Microsoft Corporation, WA, USA), and GCaMP imaging activity peaks were smoothed and quantified in ClampFit, before being copied into GraphPad Prism 9 (GraphPad Software) for statistical analysis. Normality was tested using the Shapiro-Wilk test, with further analysis conducted according to the nature of the distribution. Specifically, differences between two groups of normally distributed data for crawling velocity, recovery time from electroshock, change in aCC evoked action potential firing frequency in response to premotor interneuron stimulation and mini amplitude or frequency, were analysed by student's t-tests and are shown as mean ± SEM. Normally distributed data compared across three groups (e.g., all experiments that showed rescue of activity imbalance by ch stimulation, besides synchronicity (see below) was analysed using one-way ANOVA with multiple comparisons. Data for rescue of synchronicity following exposure to PTX by ch stimulation were not normally distributed, so were analysed using one-way ANOVA with Kruskall-Wallis multiple comparisons test. p values < 0.05 were considered significant, and levels of significance were represented by: * = $p < 0.05$, ** = $p < 0.01$, *** = $p < 0.01$.

Effect size (Cohen's d) for change in aCC evoked action potential firing frequency in response to premotor interneuron stimulation was calculated manually, using the formula: $Cohen's\ d = (M_1 - M_2)/SD_{pooled}$, where: M_1 = mean aCC action potential firing frequency before activation of premotor neuron; M_2 = mean aCC action potential firing frequency during activation of premotor neuron; $SD_{pooled} = \sqrt{((SD_1^2 + SD_2^2)/2}$.

Acknowledgements

This work was supported by funding from a Joint Wellcome Trust investigator award to R.A.B. and M.L. (Grant 217099/Z/19/Z). Work on this project benefited from the Manchester Fly Facility, established through funds from the University and the Wellcome Trust (Grant 087742/Z/08/Z).

Competing Interests

The authors declare no competing interests.

Author Contributions Statement

I.H., B.C., T.P., M.L. and R.A.B. designed research; I.H., B.C., T.P., J.J.D. and J.P. performed research; I.H., B.C., T.P., J.J.D. and J.P. analysed data; I.H. wrote the manuscript; M.L. and R.A.B. provided feedback on and edited drafts.

References

Allene, C., Cattani, A., Ackman, J. B., Bonifazi, P., Aniksztejn, L., Ben-Ari, Y. and Cossart, R. (2008) 'Sequential Generation of Two Distinct Synapse-Driven Network Patterns in Developing Neocortex', *Journal of Neuroscience,* 28(48), pp. 12851-12863.

Baines, R. A. and Bate, M. (1998) 'Electrophysiological development of central neurons in the Drosophila embryo', *Journal of Neuroscience,* 18(12), pp. 4673-4683.

Baines, R. A. and Pym, E. C. G. (2006) 'Determinants of electrical properties in developing neurons', *Seminars in Cell & Developmental Biology,* 17(1), pp. 12-19.

Bekkers, J. M. and Clements, J. D. (1999) 'Quantal amplitude and quantal variance of strontium-induced asynchronous EPSCs in rat dentate granule neurons', *Journal of Physiology-London,* 516(1), pp. 227-248.

Ben-Ari, Y. (2002) 'Excitatory actions of GABA during development: The nature of the nurture', *Nature Reviews Neuroscience,* 3(9), pp. 728-739.

Carreira-Rosario, A., York, R. A., Choi, M., Doe, C. Q. and Clandinin, T. R. (2021) 'Mechanosensory input during circuit formation shapes Drosophila motor behavior through patterned spontaneous network activity', *Current Biology,* 31(23), pp. 5341-+.

Coulson, B., Hunter, I., Doran, S., Parkin, J., Landgraf, M. and Baines, R. 2022. Critical periods in Drosophila neural network development: Importance to network tuning and therapeutic potential. Frontiers in Physiology.

Crisp, S., Evers, J. F., Fiala, A. and Bate, M. (2008) 'The development of motor coordination in Drosophila embryos', *Development,* 135(22), pp. 3707-3717.

Crisp, S. J., Evers, J. F. and Bate, M. (2011) 'Endogenous Patterns of Activity Are Required for the Maturation of a Motor Network', *Journal of Neuroscience,* 31(29), pp. 10445-10450.

Fagiolini, M. and Hensch, T. K. (2000) 'Inhibitory threshold for critical-period activation in primary visual cortex', *Nature,* 404(6774), pp. 183-186.

Fushiki, A., Kohsaka, H. and Nose, A. (2013) 'Role of Sensory Experience in Functional Development of Drosophila Motor Circuits', *Plos One,* 8(4).

Gervain, J., Vines, B. W., Chen, L. W., Seo, R. J., Hensch, T. K., Werker, J. F. and Young, A. H. 2013. Valproate reopens critical-period learning of absolute pitch. Frontiers in Systems Neuroscience.

Giachello, C. N. G. and Baines, R. A. (2015) 'Inappropriate Neural Activity during a Sensitive Period in Embryogenesis Results in Persistent Seizure-like Behavior', *Current Biology,* 25(22), pp. 2964-2968.

Giachello, C. N. G., Fan, Y. N., Landgraf, M. and Baines, R. A. (2021) 'Nitric oxide mediates activity-dependent change to synaptic excitation during a critical period in Drosophila', *Scientific Reports,* 11(1).

Giachello, C. N. G., Hunter, I., Pettini, T., Coulson, B., Knufer, A., Cachero, S., Winding, M., Zarin, A. A., Kohsaka, H., Fan, Y. N., Nose, A., Landgraf, M. and Baines, R. A. (2022) 'Electrophysiological Validation of Monosynaptic Connectivity between Premotor Interneurons and the aCC Motoneuron in the Drosophila Larval CNS', *Journal of Neuroscience,* 42(35), pp. 6724-6738.

Golovin, R. M., Vest, J., Vita, D. J. and Broadie, K. (2019) 'Activity-Dependent Remodeling of Drosophila Olfactory Sensory Neuron Brain Innervation during an Early-Life Critical Period', *Journal of Neuroscience,* 39(16), pp. 2995-3012.

Hasegawa, E., Truman, J. W. and Nose, A. (2016) 'Identification of excitatory premotor interneurons which regulate local muscle contraction during Drosophila larval locomotion', *Scientific Reports,* 6.

Hensch, T. K. (2005) 'Critical period plasticity in local cortical circuits', *Nature Reviews Neuroscience,* 6(11), pp. 877-888.

Hensch, T. K. and Bilimoria, P. M. 2012. Re-opening Windows: Manipulating Critical Periods for Brain Development. Cerebrum.

Hooks, B. M. and Chen, C. F. (2020) 'Circuitry Underlying Experience-Dependent Plasticity in the Mouse Visual System', *Neuron,* 106(1), pp. 21-36.

Hubel, D. H. and Wiesel, T. N. (1970) 'PERIOD OF SUSCEPTIBILITY TO PHYSIOLOGICAL EFFECTS OF UNILATERAL EYE CLOSURE IN KITTENS', *Journal of Physiology-London,* 206(2), pp. 419-&.

Hunter, I., Coulson, B., Zarin, A. A. and Baines, R. A. 2021. The Drosophila Larval Locomotor Circuit Provides a Model to Understand Neural Circuit Development and Function. Frontiers in Neural Circuits.

Kiral, F. R., Dutta, S. B., Linneweber, G. A., Hilgert, S., Poppa, C., Duch, C., von Kleist, M., Hassan, B. A. and Hiesinger, P. R. (2021) 'Brain connectivity inversely scales with developmental temperature in Drosophila', *Cell Reports,* 37(12).

Lambo, M. E. and Turrigiano, G. G. (2013) 'Synaptic and Intrinsic Homeostatic Mechanisms Cooperate to Increase L2/3 Pyramidal Neuron Excitability during a Late Phase of Critical Period Plasticity', *Journal of Neuroscience,* 33(20), pp. 8810-8819.

LeBlanc, J. J. and Fagiolini, M. (2011) 'Autism: A "Critical Period" Disorder?', *Neural Plasticity,* 2011.

Lin, W. H., Gunay, C., Marley, R., Prinz, A. A. and Baines, R. A. (2012) 'Activity-Dependent Alternative Splicing Increases Persistent Sodium Current and Promotes Seizure', *Journal of Neuroscience,* 32(21), pp. 7267-7277.

Lybrand, Z. R., Goswami, S., Zhu, J. F., Jarzabek, V., Merlock, N., Aktar, M., Smith, C., Zhang, L., Varma, P., Cho, K. O., Ge, S. Y. and Hsieh, J. (2021) 'A critical period of neuronal activity results in aberrant neurogenesis rewiring hippocampal circuitry in a mouse model of epilepsy', *Nature Communications,* 12(1).

Maffei, A., Nelson, S. B. and Turrigiano, G. G. (2004) 'Selective reconfiguration of layer 4 visual cortical circuitry by visual deprivation', *Nature Neuroscience,* 7(12), pp. 1353-1359.

Marley, R. and Baines, R. A. (2011a) 'Increased persistent Na+ current contributes to seizure in the slamdance bang-sensitive Drosophila mutant', *Journal of Neurophysiology,* 106(1), pp. 18-29.

Marley, R. and Baines, R. A. (2011b) 'Whole-cell patch recording from Drosophila larval neurons', *Cold Spring Harbor protocols,* 2011(9).

Nakamura, M., Valerio, P., Bhumika, S. and Barkat, T. R. (2020) 'Sequential Organization of Critical Periods in the Mouse Auditory System', *Cell Reports,* 32(8).

Ohyama, T., Schneider-Mizell, C. M., Fetter, R. D., Aleman, J. V., Franconville, R., Rivera-Alba, M., Mensh, B. D., Branson, K. M., Simpson, J. H., Truman, J. W., Cardona, A. and Zlatic, M. (2015) 'A multilevel multimodal circuit enhances action selection in Drosophila', *Nature,* 520(7549), pp. 633-U107.

Pulver, S. R., Bayley, T. G., Taylor, A. L., Berni, J., Bate, M. and Hedwig, B. (2015) 'Imaging fictive locomotor patterns in larval Drosophila', *Journal of Neurophysiology,* 114(5), pp. 2564-2577.

Reh, R. K., Dias, B. G., Nelson, C. A., Kaufer, D., Werker, J. F., Kolb, B., Levine, J. D. and Hensch, T. K. (2020) 'Critical period regulation across multiple timescales', *Proceedings of the National Academy of Sciences of the United States of America,* 117(38), pp. 23242-23251.

Scheffer, L. K. and Xu, C. S. and Januszewski, M. and Lu, Z. Y. and Takemura, S. Y. and Hayworth, K. J. and Huang, G. B. and Shinomiya, K. and Maitlin-Shepard, J. and Berg, S. and Clements, J. and Hubbard, P. M. and Katz, W. T. and Umayam, L. and Zhao, T. and Ackerman, D. and Blakely, T. and Bogovic, J. and Dolafi, T. and Kainmueller, D. and Kawase, T. and Khairy, K. A. and Leavitt, L. and Li, P. H. and Lindsey, L. and Neubarth, N. and Olbris, D. J. and Otsuna, H. and Trautman, E. T. and Ito, M. and Bates, A. S. and Goldammer, J. and Wolff, T. and Svirskas, R. and Schlegel, P. and Neace, E. and Knecht, C. J. and Alvarado, C. X. and Bailey, D. A. and Ballinger, S. and Borycz, J. A. and Canino, B. S. and Cheatham, N. and Cook, M. and Dreher, M. and Duclos, O. and Eubanks, B. and Fairbanks, K. and Finley, S. and Forknall, N. and Francis, A. and Hopkins, G. P. and Joyce, E. M. and Kim, S. and Kirk, N. A. and Kovalyak, J. and Lauchie, S. A. and Lohff, A. and Maldonado, C. and Manley, E. A. and McLin, S. and Mooney, C. and Ndama, M. and Ogundeyi, O. and Okeoma, N. and Ordish, C. and Padilla, N. and Patrick, C. M. and Paterson, T. and Phillips, E. E. and Phillips, E. M. and Rampally, N. and Ribeiro, C. and Robertson, M. K. and Rymer, J. T. and Ryan, S. M. and Sammons, M. and Scott, A. K. and Scott, A. L. and Shinomiya, A. and Smith, C. and Smith, K. and Smith, N. L. and Sobeski, M. A. and Suleiman, A. and Swift, J. and Takemura, S. and Talebi, I. and Tarnogorska, D. and Tenshaw, E. and Tokhi, T. and Walsh, J. J. and Yang, T. and Horne, J. A. and Li, F. and Parekh, R. and Rivlin, P. K. and Jayaraman, V. and Costa, M. and Jefferis, G. and Ito, K. and Saalfeld, S. and George, R. and Meinertzhagen, I. A. and Rubin, G. M. and Hess, H. F. and Jain, V. and Plaza, S. M. (2020) 'A connectome and analysis of the adult Drosophila central brain', *Elife,* 9.

Schneider-Mizell, C. M., Gerhard, S., Longair, M., Kazimiers, T., Li, F., Zwart, M. F., Champion, A., Midgley, F. M., Fetter, R. D., Saalfeld, S. and Cardona, A. (2016) 'Quantitative neuroanatomy for connectomics in Drosophila', *Elife,* 5.

Selemon, L. D. and Zecevic, N. (2015) 'Schizophrenia: a tale of two critical periods for prefrontal cortical development', *Translational Psychiatry,* 5.

Streit, A. K., Fan, Y. N., Masullo, L. and Baines, R. A. (2016) 'Calcium Imaging of Neuronal Activity in Drosophila Can Identify Anticonvulsive Compounds', *Plos One,* 11(2).

Styr, B., Gonen, N., Zarhin, D., Ruggiero, A., Atsmon, R., Gazit, N., Braun, G., Frere, S., Vertkin, I., Shapira, I., Harel, M., Heim, L. R., Katsenelson, M., Rechnitz, O., Fadila, S., Derdikman, D., Rubinstein, M., Geiger, T., Ruppin, E. and Slutsky, I. (2019) 'Mitochondrial Regulation of the Hippocampal Firing Rate Set Point and Seizure Susceptibility', *Neuron,* 102(5), pp. 1009-+.

Tien, N. W. and Kerschensteiner, D. (2018) 'Homeostatic plasticity in neural development', *Neural Development,* 13.

Tran, H. T., Li, Y. C., Lin, H. Y., Lee, S. D. and Wang, P. J. (2022) 'Sensory Processing Impairments in Children with Developmental Coordination Disorder', *Children-Basel,* 9(10).

Truszkowski, T. L. S. and Aizenman, C. D. (2015) 'Neurobiology: Setting the Set Point for Neural Homeostasis', *Current Biology,* 25(23), pp. R1132-R1133.

Wong-Riley, M. T. T. (2021) 'The critical period: neurochemical and synaptic mechanisms shared by the visual cortex and the brain stem respiratory system', *Proceedings of the Royal Society B-Biological Sciences,* 288(1958).

Xu-Friedman, M. A. and Regehr, W. G. (1999) 'Presynaptic strontium dynamics and synaptic transmission', *Biophysical Journal,* 76(4), pp. 2029-2042.

Zarin, A. A., Mark, B., Cardona, A., Litwin-Kumar, A. and Doe, C. Q. (2019) 'A multilayer circuit architecture for the generation of distinct locomotor behaviors in Drosophila', *Elife,* 8.

Zeng, X. S. Z., Komanome, Y., Kawasaki, T., Inada, K., Jonaitis, J., Pulver, S. R., Kazama, H. and Nose, A. (2021) 'An electrically coupled pioneer circuit enables motor development via proprioceptive feedback in Drosophila embryos', *Current Biology,* 31(23), pp. 5327-+.

Zheng, Z. H., Lauritzen, J. S., Perlman, E., Robinson, C. G., Nichols, M., Milkie, D., Torrens, O., Price, J., Fisher, C. B., Sharifi, N., Calle-Schuler, S. A., Kmecova, L., Ali, I. J., Karsh, B., Trautman, E. T., Bogovic, J. A., Hanslovsky, P., Jefferis, G., Kazhdan, M., Khairy, K., Saalfeld, S., Fetter, R. D. and Bock, D. D. (2018) 'A Complete Electron Microscopy Volume of the Brain of Adult Drosophila melanogaster', *Cell,* 174(3), pp. 730-+.

Supplementary Information

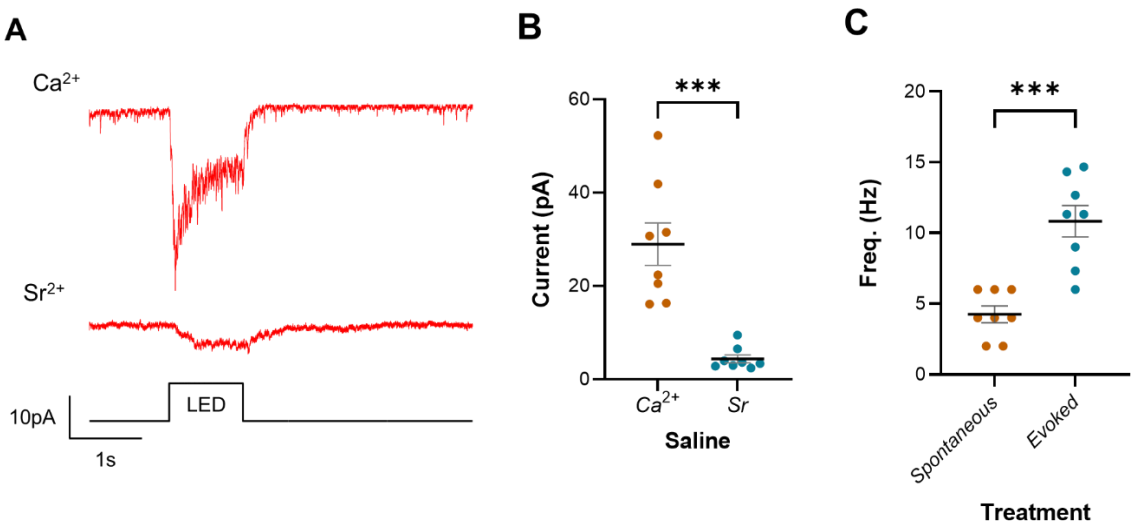

Figure S1: Optogenetic activation of A18a in 6mM Sr^{2+} saline stimulates asynchronous release of minis. (A) Representative traces show synaptic currents recorded in aCC following optogenetic stimulation (1s LED) of A18a in control (Ca^{2+}) or 6mM Sr^{2+} saline. Recordings made in control saline feature large synaptic events (~30pA), indicative of normal vesicular release from the premotor. By contrast, the large current response to optogenetic stimulation is absent in 6mM Sr^{2+}. (B) Analysis of peak currents recorded in aCC, elicited by optogenetic stimulation of A18a are significantly larger in control (Ca^{2+}) than 6mM Sr^{2+} saline (28.96 ± 4.56s, Ca^{2+}; 4.4 ± 0.85s, Sr^{2+}; n = 8, 8; $p < 0.0001$), thus, the changes we observed in current amplitude are consistent with the asynchronous mini release reported when using Sr^{2+} saline in mammals (Xu-Friedman and Regehr, 1999; Bekkers and Clements, 1999). (C) Similarly, there is a significant increase in the frequency of asynchronous synaptic events (minis) recorded in aCC in 6mM Sr^{2+} saline, in the 3s following stimulation of A18a (Evoked) versus the 3s prior (4.25 ± 0.59Hz, Spontaneous; 10.83 ± 1.12Hz, Evoked; n = 8, 8; $p < 0.0001$). In combination, these results suggest recording current in aCC following optogenetic stimulation of A18a in 6mM Sr^{2+} saline, enables quantifying the frequency and amplitude of minis elicited by this premotor interneuron.

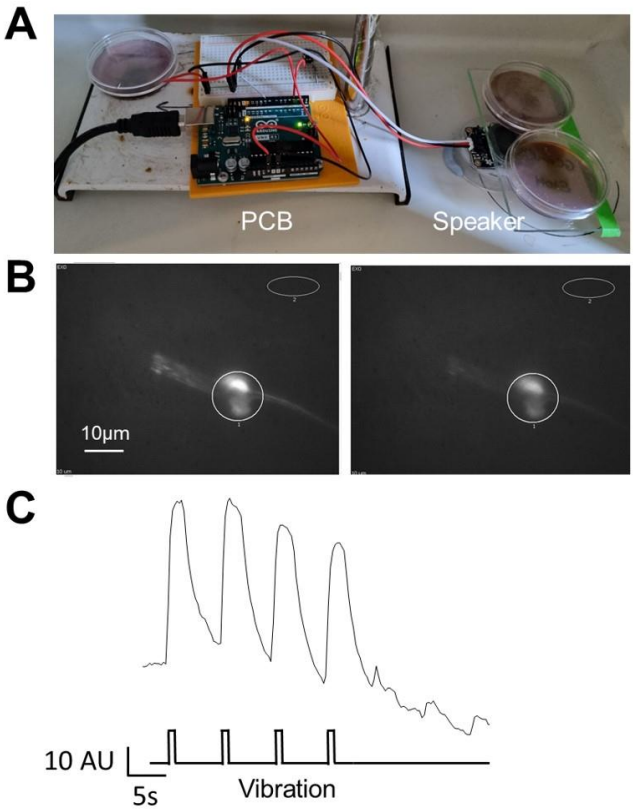

Figure S2: A custom-built device provides mechanical stimulation of chordotonal neurons. (A) image of the device, showing an Arduino Uno Rev 3 printed circuit board with microcontroller, that drives a speaker according to timings and frequency (i.e., 17-19h AEL at 0.5Hz) coded using C^{++} in Arduino IDE, and with an amplitude adjusted using a potentiometer. (B) GCaMP imaging demonstrating activity in the chordotonal neurons prior to (left) and following (right) stimulation by the device (response shown is to 1s tone at 80dB). (C) Representative trace of the activity shown in (B).